https://doi.org/10.5194/acp-2020-1169
Preprint. Discussion started: 24 November 2020

Atmospheric Chemistry and Physics Discussions

Mobile monitoring of urban air quality at high spatial resolution by low-cost sensors: Impacts of COVID-19 pandemic lockdown

Shibao Wang[1], Yun Ma[1], Zhongrui Wang[1], Lei Wang[1], Xuguang Chi[1], Aijun Ding[1], Mingzhi Yao[2], Yunpeng Li[2], Qilin Li[2], Mengxian Wu[3], Ling Zhang[3], Yongle Xiao[3], Yanxu Zhang[1]

[1]School of Atmospheric Sciences, Nanjing University, Nanjing, China
[2]Beijing SPC Environment Protection Tech Company Ltd., Beijing, China
[3]Hebei Saihero Environmental Protection Hi-tech. Company Ltd., Shijiazhuang, China

Correspondence to: Yanxu Zhang (zhangyx@nju.edu.cn)

Abstract. The development of low-cost sensors and novel calibration algorithms provides new hints to complement conventional ground-based observation sites to evaluate the spatial and temporal distribution of pollutants on hyperlocal scales (tens of meters). Here we use sensors deployed on a taxi fleet to explore the air quality in the road network of Nanjing over the course of a year (Oct. 2019 – Sep. 2020). Based on GIS technology, we develop a grid analysis method to obtain 50 m resolution maps of major air pollutants (CO, NO_2, and O_3). Through hotspots identification analysis, we find three main sources of air pollutants including traffic, industrial emissions, and cooking fumes. We find that CO and NO_2 concentrations show a pattern: highways > arterial roads > secondary roads > branch roads > residential streets, reflecting traffic volume. While the O_3 concentrations in these five road types are in opposite order due to the titration effect of NOx. Combined the mobile measurements and the stationary stations data, we diagnose that the contribution of traffic-related emissions to CO and NO_2 are 42.6% and 26.3%, respectively. Compared to the pre-COVID period, the concentrations of CO and NO_2 during COVID-lockdown period decreased for 44.9% and 47.1%, respectively, and the contribution of traffic-related emissions to them both decreased by more than 50%. With the end of the COVID-lockdown period, traffic emissions and air pollutant concentrations rebounded substantially, indicating that traffic emissions have a crucial impact on the variation of air pollutants levels in urban regions. This research demonstrates the sense power of mobile monitoring for urban air pollution, which provides detailed information for source attribution, accurate traceability, and potential mitigation strategies at urban micro-scale.

1 Introduction

Urban air pollution poses a serious health threat with >80% of the world's urban residents exposed to air pollution levels that exceed the World Health Organization (WHO) guidelines (WHO, 2016). The global urban air pollution also deteriorated by 8% during recent years despite improvements in some regions (WHO, 2016). Extremely large spatial variability exists for urban air pollutants [e.g., carbon monoxide (CO), nitrogen dioxide (NO_2), and ozone (O_3)] over scales from kilometer to meters, as a result of complex flow pattern, non-linear chemical reactions, and unevenly distributed emissions from vehicle and industrial activities (Apte et al., 2017; Miller et al., 2020). Here we illustrate an approach to obtain a high-resolution urban air quality map using low-cost sensors deployed on a routinely operating taxi fleet.

High spatio-temporal resolution air quality data is critical to urban air quality management, exposure assessment, epidemiology study, and environmental equity (Apte et al., 2011, 2017; Boogaard et al., 2010). Numerous methodologies have been developed to obtain urban air pollutant concentrations, including stationary monitoring networks (Cavellin et al., 2016), near-roadway sampling (Karner et al., 2010; Zhu et al., 2009; Padro-Martinez et al., 2012), satellite remote sensing (Laughner et al., 2018; Xu et al., 2019), land use regression (LUR) model (Weissert et al., 2020), and chemical transport models (CTMs) (Li et al., 2010). However, the stationary monitoring stations (including near-roadway sampling) are sparse and uneven, and the ability to reflect the details of urban air pollution is limited, especially at remote communities (Snyder et al., 2013). Remote sensing and CTMs are generally spatially coarse (~km resolution), and cannot resolve species that are inert to radiative transfer

https://doi.org/10.5194/acp-2020-1169
Preprint. Discussion started: 24 November 2020

Atmospheric Chemistry and Physics Discussions

(e.g. mercury and lead) or without known emission inventory and/or chemical mechanisms. LUR model can estimate concentrations at high spatial resolution, but it provides limited temporal information, and the predicting power is poor in areas with specific local sources (Kerckhoffs et al., 2016).

Mobile monitoring is a promising approach to garner high spatial resolution observations representative of the community scale (Miller et al., 2020; Hasenfratz et al., 2015). Different vehicle platforms are used for mobile monitoring, including minivan (Isakov et al., 2007), cargo tricycle (Airparif, 2009), bicycle (Bart et al., 2012), taxi (Le and Cha, 2018), street view cars (Apte et al., 2017), and city bus (Kaivonen and Ngai, 2020). However, the scale of deployment and subsequent data coverage are limited by the cost of the observation instrument (Bossche et al., 2015). This issue has been addressed by the development of low-cost sensors that are calibrated with machine learning based algorithms (Miskell et al., 2018; Shiva et al., 2019; Lim et al., 2019). The emergence of low-cost air monitoring technologies was recognized by the U.S. EPA (Snyder et al., 2013) and European Commission (Kaur et al., 2007), and was also recommended to be incorporated in the next Air Quality Directive (Borrego et al., 2015). For example, Weissert et al. (2020) combined land use information with low-cost sensors to obtain hourly O_3 and NO_2 concentration distributions at a resolution of 50 m. High agreements are also found between well-calibrated low-cost sensor systems and standard instrumentations (Chatzidiakou et al., 2019; Hagan et al., 2019).

The objective of this study is to illustrate the sensing power of low-cost sensors deployed on a routinely operating taxi fleet platform in a megacity. We combine mobile observations and geographic information system (GIS) to obtain the hourly distribution of multiple air pollutants at 50 m resolution. By comparing to the measurements by background sites, the contribution of traffic emission to urban air pollution is also diagnosed. We explore the influencing factors of pollutant levels including time of the day/week and holidays. Moreover, our sampling period covered the outbreak of COVID-19 in China. The pandemic lockdown had a tremendous impact on the socio-economic activities especially the traffic sector, and subsequently the air quality (Zhang et al., 2020; Huang et al., 2020). We evaluate how urban air quality changes at different periods of the pandemic and explore the impact of traffic-related emissions.

2 Material and methods

2.1 Mobile monitoring

We use the mobile sampler XHAQSN-508 from Hebei Sailhero Environmental Protection High-tech Co., Ltd. (Hebei, China) to measure the air quality in Nanjing urban area. The instrument is equipped with internal gas sensors for CO, NO_2, and O_3 (dimensions: 290×81×55 mm; weight: 1.0 kg) and is fixed in the top lamp support pole (~1.5 m above ground) of two Nanjing taxis (Figure 1). This device integrates components for data integration, processing, and transmission, and provides data management, quality control, and visualization functions. The monitoring system is configured to continuous measure at a frequency of once per 10 seconds. Taxis fueled with electricity and liquefied natural gas are selected to reduce the impact of emissions from the sampling vehicles themselves. We continuously measured the concentration of CO, NO_2, and O_3 in the street canyon in the urban area of Nanjing (with the center located at 32.07 °N and 118.72 °E) for a whole year (Oct 1, 2019 - Sep 30, 2020). The sampling routes were relatively random during taxi operations, mainly on the arterial roads. Generally, the sampling campaign is conducted on both weekdays and weekends from 6:00 A.M. to 10:00 P.M. Occasionally the taxi drivers work for the night shift, and the instruments are run from 10:00 P.M. to 6:00 A.M. The collected data covers 373 km^2 with a population of 6 million (Figure 1).

https://doi.org/10.5194/acp-2020-1169
Preprint. Discussion started: 24 November 2020

Atmospheric Chemistry and Physics Discussions

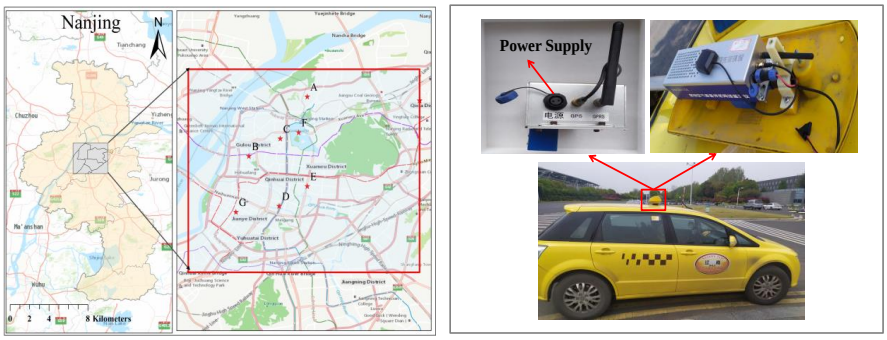

Figure 1. Location of the monitoring areas in the city of Nanjing (left) and photo of instrument installment (right). Red stars are the locations of stationary stations belonging to the national air quality measurement network of China. These stations cover different functional regions of the city: A, B, C, D, E, F, and G represent industrial, cultural and educational, commercial, traffic, residential, ecological park and new urban area, respectively. Map credit: ESRI 2020.

2.2 Sensors calibration and validation

The XHAQSN-508 is calibrated once per month. The instrument is placed at the SORPES superstation in the Xianlin Campus of Nanjing University (https://as.nju.edu.cn/as_en/obsplatform/list.html) for at least seven days. The collected data is calibrated against standard instruments (Thermo Fisher Scientific 48i, 42i, and 49i, USA for CO, NO_2, and O_3, respectively) (Ding et al., 2013). During the monitoring campaign, if the data deviated substantially from the nearest national network stations (shown as red stars in Figure 1 left), the instrument is also taken offline and re-calibrated. A supervised machine learning methodology based on the Gradient Boost Decision Tree (GBDT) is used for data calibration (Johnson et al., 2018). The raw signals of sensors are used as input data, and the stationary instrument data are training targets. The parameters of the machine learning model are adjusted continuously based on gradient descent algorithm. The R^2 of the calibration results are generally high (> 0.90) for all the three air pollutants (e.g. Figure 2a).

We use a calibration-validation methodology to evaluate the performance of the calibrated sensors (Chatzidiakou et al., 2019). This method includes two phases: first, the sampler was calibrated against the SORPES station for 10 days (Jun. 1-10, 2020), and the sensor data were used for sensor algorithm training as above described (Figure 2a); second, we continued to place the sampler in the station (Jun. 11-17, 2020). However, the sensor data are not used for calibration but directly fed in the algorithm trained in the first phase. The results are compared with the station data (i.e. validation phase, Figure 2b). We find that the sensor data agree well with standard instrumentation in the second phase. The sensor retrieved CO, NO_2, and O_3 concentrations are 0.58±0.12 mg/m^3, 8.40±4.30 μg/m^3, 27.3±16.5 μg/m^3 respectively, not significantly different from that by standard instruments (0.50±0.10 mg/m^3 and 10.5±6.31 μg/m^3, and 32.4±20.2 μg/m^3) (α = 0.05, ANOVA analysis). The R^2 values remain generally high (0.82-0.97) for different air pollutants (CO and O_3) except NO_2 (R^2 = 0.67). The lower R^2 value for NO_2 may be associated with the higher humidity during the validation period (Jun. 13-16, 2020). As NO_2 is water dissolvable, high humidity may lead to a low bias for sensors (Wei et al., 2018). Field calibration of low-cost sensors is still a challenging task, as it is greatly affected by atmospheric composition and meteorological conditions (Spinelle et al., 2017; Castell et al. 2017). Our results have high R^2 values compared to previous studies, indicating relatively high accuracy (e.g. Castell et al. 2017). The results from the two sensors also agree with each other reasonably well, with R^2 values ranged 0.97-0.99 for a linear regression. Their data are thus combined in the following analysis to achieve a maximum data coverage.

https://doi.org/10.5194/acp-2020-1169
Preprint. Discussion started: 24 November 2020

Atmospheric Chemistry and Physics Discussions

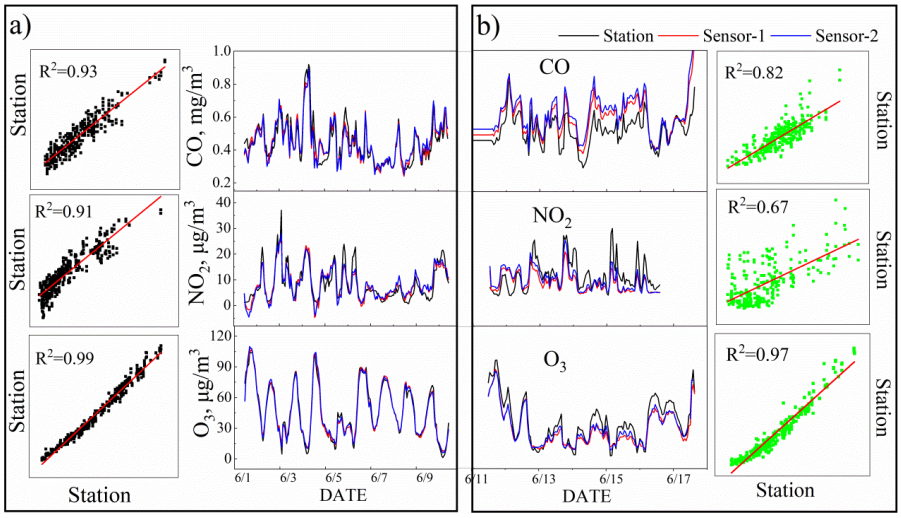

Figure 2. Sensor performance evaluated by a calibration-validation methodology for CO, NO_2, and O_3. a) calibration period (Jun 1-10, 2020); b) validation period (Jun 11-17, 2020). The time series plots compare the concentrations measured by the co-located sensors and standard instruments, while the scatterplots show linear regressions between them.

2.3 Data processing

As the mobile monitoring platform samples along the trajectories of carrying vehicles, we need to either sacrifice the temporal information to calculate the spatial distribution of air pollutants, or the spatial information to temporal variations. Similar approaches have also been adopted by previous studies (Bossche et al., 2015; Apte et al., 2017; Farrell et al. 2015). To generate the spatial distribution of air pollutants at high spatial resolution, we divide the research area into grids with 50 m × 50 m resolution, and calculate the mean values of the samples collected in each grid. Similarly, we average all the samples collected in different grids but in the same hour of the day to get hourly mean concentrations of the sampling domain. The GPS signal is missing when the taxis pass through the nine underground tunnels in Nanjing (e.g. Xuanwu lake tunnel and Jiuhuashan tunnel in the city center, Figure 3). We assume the taxies travel in a constant speed and the sampling points are uniformly allocated along the tunnel. We use the Arcgis 10.2 software for data processing. To calculate the air pollutants concentrations (CO, NO_2, and O_3) map of different road types and the contribution of traffic emissions to them, we divided the urban roads in Nanjing urban area into five types (https://wiki.openstreetmap.org/wiki/Key:highway), including highways, arterial roads, secondary roads, branch roads, and residential streets. Roads and land use data of Nanjing shown in Figure 3 are based on OpenStreetMap (OpenStreetMap contributors, 2020).

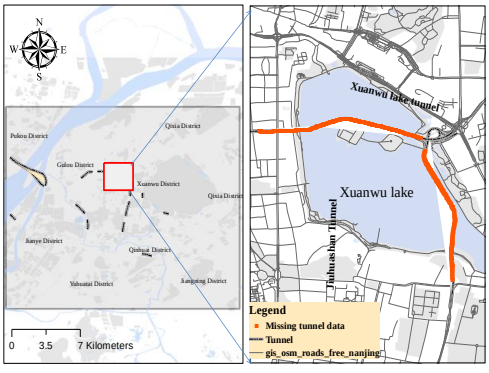

Figure 3. Locations of tunnels in Nanjing urban area. © OpenStreetMap contributors 2019. Distributed under a Creative Commons BY-SA License.

https://doi.org/10.5194/acp-2020-1169
Preprint. Discussion started: 24 November 2020

Atmospheric Chemistry and Physics Discussions

2.4 Traffic source attribution

The mobile platform keeps sampling in the urban road network which carries a strong signal from traffic sources. By contrast, stationary stations are often located far away from major roads to represent a regional background air pollution level (Hilker et al., 2019). Therefore, the contribution from traffic-related emissions can be obtained by differencing the mobile measurements and the stationary ones, following Bossche et al. (2015):

$$AP_{traffic,ij} = (AP_{ij} - AP_{min})/AP_{ij} \quad (1)$$

where, $AP_{traffic,ij}$ represents the air pollutant concentration contributed by traffic emissions for the i^{th} pollutant at time j, %; AP_{ij} is the sensor measured air pollutant concentration; and AP_{min} means the ambient background concentration, which is calculated as the minimum of the measurements from all the stations in Nanjing in the national air quality network without major sources within a direct vicinity of 50 m (https://quotsoft.net/air/, Figure 1). We refer to this method as "background site (BS)".

We also adopt a method similar to Apte et al. (2017) for traffic source attribution. This method includes a peak detection algorithm to calculate the contribution of local traffic emission sources to on-road pollutant concentrations. We calculate the mean and minimum of air pollutant concentrations in each grid as the "peak" and "baseline", respectively. The difference between the two is considered as the contribution from traffic sources. We refer to this method as "peak detection (PD)". Matlab 2019b is used for such data calculation.

3 Results and discussion

3.1 Effect of spatial resolution on reproducibility

There is a trade-off between the resolution of air pollutant concentration map and its reproducibility, i.e. high-resolution maps subject to large randomness due to the limited number of samples in each grid. We investigate the consistency of spatial patterns of different resolution (10-100 m). We calculate the domain-averaged standard error of the means of samples in each grid (SEM):

$$SEM = \overline{\sigma/\sqrt{n}} \quad (2)$$

where, σ and n are the standard deviation and number of samples in each grid, respectively. We find the calculated SEM first decays rapidly with the grid spacing but tends to be in a regime of linear decay after a resolution of approximately 50 m for all the three air pollutants (Figure 4). Therefore, we choose a resolution of 50 m, which is consistent with previous studies (Bossche et al. 2015; Apte et al. 2017). For example, Bossche et al. (2015) used a spatial resolution of 20-50 m to map urban air quality and identify hotspots. Apte et al. (2017) found that reproducible results (with high precision and low bias) of NO, NO_2, and black carbon can be generated by at least 10-25 repetitions in a specific area with 30 m median spatial aggregation.

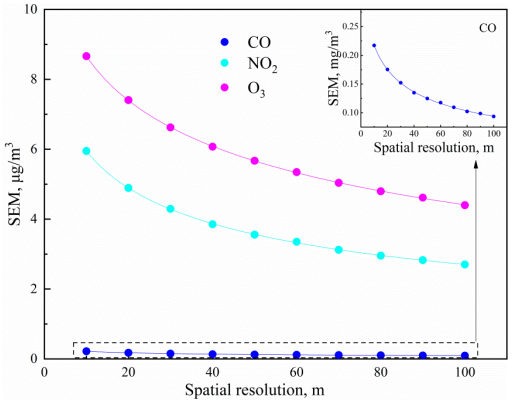

https://doi.org/10.5194/acp-2020-1169
Preprint. Discussion started: 24 November 2020

Atmospheric Chemistry and Physics Discussions

Figure 4. Relationship between grid resolution and the domain-averaged standard error of the mean of samples in each grid (SEM) for CO, NO_2, and O_3.

3.2 Road network coverage

A total of 1.32 million pieces of data were obtained during the observation period, which covers 66.4% of the major roads in Nanjing in the sampling domain with a large repeat-visit frequency [median repetition = 61 (14 and 264 as the lower and upper quartiles, respectively, the same hereinafter)] (Figure 5a). The type of road with the most visits is the Neihuan lines [258 (116, 526)], followed by the arterial roads [125 (35, 393)], secondary roads [151 (24, 442)], and highways [34 (12, 115)]. The residential streets [22 (6, 100)] have the least visits.

Apart from the areas without roads, such as the Yangtze River, Xuanwu Lake, and Purple Mountain, the data covers 43.5% of the 50-m grids in the research area with the two taxis contributing 36.8% and 37.2%. As shown in Fig 5b, the median number of repeated frequency in each grid is 66 (18, 286), with the highest value of 15449 in Nanjing South Railway Station and the lowest in some residential roads (1). The repeated frequencies in each 50-m grid along the arterial roads and Neihuan line are higher than other types of roads, i.e. Zhongyang road, Huju road, Neihuandong and Neihuanxi lines (Figure 5b). Our repeated frequency is generally higher than previous research on mobile monitoring of urban air pollution (Peters et al., 2013; Poppel et al., 2013; Bossche et al., 2015; Apte at al., 2017), which can lower the uncertainty of our results.

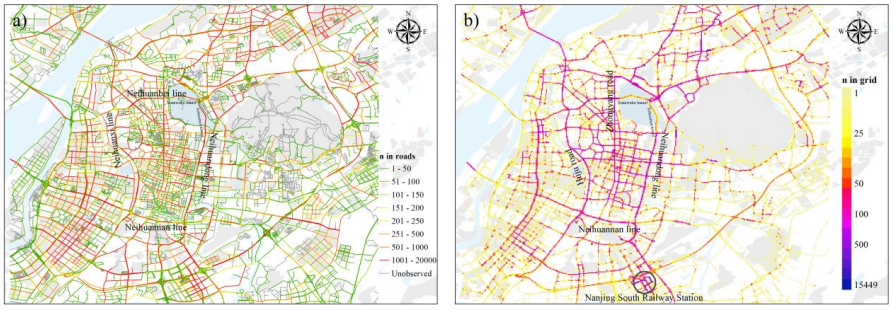

Figure 5. Mobile monitoring data coverage with regard to road (a) and 50 m grid (b). © OpenStreetMap contributors 2019. Distributed under a Creative Commons BY-SA License.

3.3 Uncertainty analysis

Figure 6 shows the coefficients of variation (CV≡standard deviation/ mean×100%) for different air pollutants in each grid. For one thing, this matric quantifies the sensing power of mobile monitoring, i.e. more data points reduce uncertainty of observations. For another, it reflects the inherent variability of pollutants caused by factors such as meteorological conditions and hotspots emission sources. We find that the CV values are lower than 100% on the main roads, including highways and arterial roads, but higher than 100% on some tunnel and residential streets. As discussed above, the road network coverage is much higher over the main roads than smaller roads. This indicates that increasing the sampling numbers within secondary and residential roads is the most useful to reduce the uncertainty of mobile observation. It is also interesting to notice that a single taxi has a data coverage of ~37% but the second one only increases it by ~6% to 43.5%, which implies that the marginal increase of spatial coverage decreases substantially with increasing number of sensors. This is indeed one limitation of our monitoring platform, and much larger fleet size or different sampling platforms (e.g. bikes) may be needed to reduce the uncertainty over these smaller roads.

Although the spatial patterns of CV are similar for different air pollutants, we find generally higher CV for O_3 (67.3%) and NOx (59.5%) than CO (51.6%). This is associated with the spatial and temporal variability of different air pollutants, which is mainly influenced by their lifetimes in the atmosphere. The chemical properties of CO are the most stable in the environment (τ = 1~2 months), and its spatial concentration difference is more affected by the sampling time and the number

https://doi.org/10.5194/acp-2020-1169
Preprint. Discussion started: 24 November 2020

Atmospheric Chemistry and Physics Discussions

of samples. The lifetime of NOx is shorter (τ = 2~11 hours, Romer et al., 2016), so the measured concentrations are more influenced by local or "hotspot" emissions and meteorological factors. O_3 has the shortest lifetime (τ = ~1 hour in urban atmosphere, McClurkin et al., 2013) among the three pollutants. The level of ozone is affected by its precursors (NO_2 and VOCs), which both have large variability (Sharma et al., 2016). The complex chemical reactions also increase its spatial heterogeneity.

Figure 6. Spatial distribution of coefficient of variation for multi-pollutants in 50 m grids in research domain. © OpenStreetMap contributors 2019. Distributed under a Creative Commons BY-SA License.

3.4 Spatial distribution

3.4.1 Hotspots identification

Although the instantaneous pollution level varies drastically in different road environments, we obtain a relatively robust time integrated pollution estimate by calculating the mean of repeatedly samples (Figure 7). We define the area where the pollutant concentrations are 50% higher than nearby grids (radius = 300 m) as "hotspots" following Apte et al., (2017). A total of 14 hotspots are identified, and the specific information is shown in Table 1. Most of the "hotspots" show relatively apparent spatial "peaks" for multiple pollutants.

We find that "hotspots" are mainly affected by one of the three types of emission sources, namely traffic emissions (diesel and gasoline on-road vehicle exhaust), industrial emissions, and cooking fumes. The mean CO and NO_2 concentrations are relatively high at the crossroads (E, 1.97 mg/m^3 and 34.8 μg/m^3), tunnels (B, 1.74 mg/m^3 and 35.6 μg/m^3, respectively), the roads near the hospital (M, 1.16 mg/m^3 and 34.7 μg/m^3), and near the railway station (A, 1.10 mg/m^3 and 23.0 μg/m^3), which are affected by on-road traffic emissions. In addition, due to the construction of Maigaoqiao subway station (L, 1.41 mg/m^3 and 30.8 μg/m^3), diesel vehicles and off-road traffic emission also make a great contribution to CO and NO_2 concentrations. Industrial emissions from petrochemical enterprises (N) also lead to high NO_2 concentrations (0.26 - 112 μg/m^3) on surrounding roads.

As the traffic and industrial sources contribute significantly to the precursors of O_3 (NOx and VOC), the mean O_3 concentration is the highest near the subway entrance (C, 41.7 μg/m^3), followed by the memorial hall in Nanjing (K, 39.8 μg/m^3), high-tech development zones (D, 33.2 μg/m^3), Olympic Sports Center (J, 30.6 μg/m^3), and residential area (F, 30.4 μg/m^3). Taxi sensor data also reveals the secondary pollution characteristics in micro scales, showing that O_3 concentration in the downtown area with dense buildings is significantly higher than that in other areas, especially some residential areas in Jianye and Gulou district. Previous studies have also found that the air pollutants "hotspots" are associated with traffic-related emissions [e.g., heavy-duty diesel vehicles (Targino et al., 2016) and vehicle congestion (Gately et al., 2017)] and high-density urban areas (Li et al. 2018). These identified air pollution "hotspots" and the diagnosed source contributions provide helpful information for urban air quality management, which demonstrates the sensing power of mobile monitoring deployed on taxi fleet.

https://doi.org/10.5194/acp-2020-1169
Preprint. Discussion started: 24 November 2020

Atmospheric Chemistry and Physics Discussions

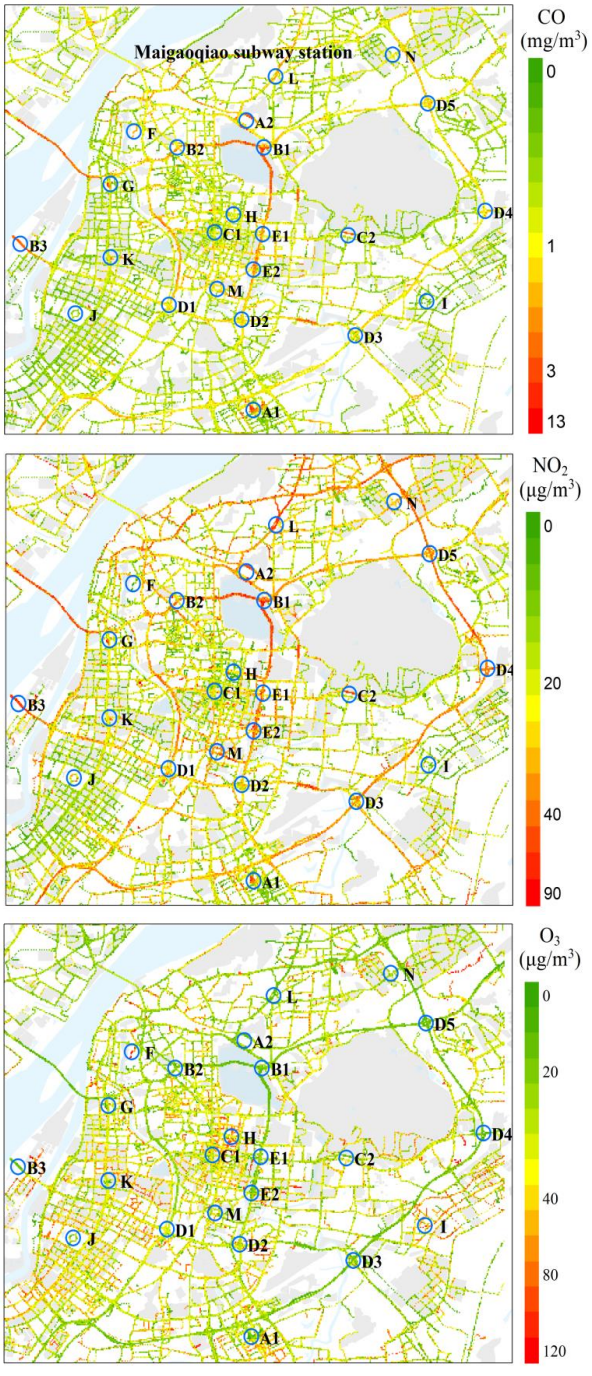

225 **Figure 7.** Spatial distribution and "hotspots" of air pollutant concentrations in the research domain (CO, NO_2, and O_3). Circles marked with A-N represent the identified "hotspots", where the air pollutants concentrations are at least 50% higher than the surrounding area (300 m radius). © OpenStreetMap contributors 2019. Distributed under a Creative Commons BY-SA License.

Table 1. "Hotspots" of air pollution for multi-pollutants identified in Nanjing.

https://doi.org/10.5194/acp-2020-1169
Preprint. Discussion started: 24 November 2020

Atmospheric Chemistry and Physics Discussions

ID	Specific	No	CO, mg/m^3	NO_2, μg/m^3	O_3, μg/m^3	Description/Potential sources
A	A1,A2	6535	1.10±0.82	23.0±15.9	30.3±24.2	Nanjing railway station, gasoline vehicle emission
B	B1,B2,B3	4177	1.74±1.74	35.6±26.1	19.4±18.3	Exit and entrance of tunnel, gasoline vehicle emission
C	C1,C2,C3	1002	1.23±0.39	19.9±12.5	41.7±27.1	Subway entrance, gasoline vehicle emission
D	D1-D6	4333	0.96±0.61	25.1±15.0	28.5±21.7	Overpass on ring road, vehicle emission
E	E1,E2	5354	1.97±3.04	34.8±26.8	20.1±19.8	Crossroads, vehicle emission
F	F	4664	0.78±0.71	21.3±16.5	30.4±21.6	Residential area, with higher H/W ratio
G	G	1052	1.05±0.53	32.5±14.2	16.7±13.6	Moonlight Plaza/ vehicle emission
H	H	92	0.69±0.11	22.1±9.79	23.2±12.9	Cooking emissions
I	I	4967	1.02±0.59	24.4±15.3	33.2±22.7	Nanjing Hi-Tech Industry Development Zone
J	J	4229	1.10±0.62	24.3±14.9	30.6±23.6	Olympic Sports Center, vehicle emission
K	K	3957	0.83±0.46	19.9±14.3	39.8±24.2	The memorial hall in Nanjing, vehicle emission
L	L	6160	1.41±1.31	30.8±21.0	25.2±21.5	Maigaoqiao subway station, diesel vehicle emission
M	M	6231	1.16±0.74	34.7±23.5	17.9±18.7	Hospital, vehicle emission
N	N	2386	0.86±0.49	24.6±14.0	25.2±20.3	Petrochemical enterprises, Industrial emissions

No: Observation points within 300 m near the hotspots.

3.4.2 Air pollutant concentrations in different types of roads

We find that air pollutant levels differ vastly among the five types of roads ($p < 0.05$, with ANOVA method). The mean CO and NO_2 concentrations follow this trend: highways (1.10±0.59 mg/m^3 and 29.2±8.66 μg/m^3, respectively) > arterial roads (0.958±0.308 mg/m^3 and 25.0±6.90 μg/m^3) > secondary roads (0.855±0.401 mg/m^3 and 21.8±8.89 μg/m^3) > branch roads (0.818±0.216 mg/m^3 and 20.3±6.79 μg/m^3) > residential streets (0.783±0.299 mg/m^3 and 19.7±8.35 μg/m^3) (Table 2). However, the mean O_3 concentrations in different types of roads are opposite to that of CO and NO_2: residential streets (35.1±15.4 μg/m^3) > branch ways (32.7±12.2 μg/m^3) > secondary roads (31.9±10.0 μg/m^3) > arterial roads (29.6±7.52 μg/m^3) > highways (23.3±9.12 μg/m^3).

The differences of air pollutant concentrations among different road types are firstly affected by the traffic-related emission sources including vehicle engine exhaust, which is a function of traffic flow and speed, vehicle type, etc. (Sahanavin et al., 2018). The general decreasing trends we observed for CO and NO_2 are consistent with traffic flow and congestion index in Nanjing urban area (Table 2, Zou et al., 2017). Apte et al. (2017) also found that the NO_2 concentration decreased in turn on highways, arterial roads and residential streets, which are in good agreement with our research. The observed O_3 concentrations have opposite trends of CO and NOx with highest concentrations in residential streets (Table 2). As O_3 production in Nanjing is in VOC-limited regions, lower NOx could reduce its titration of O_3 and subsequently increase O_3 concentrations (Ding et al., 2013; Xie et al., 2016). This indicates the necessity of VOC emission control to reduce O_3 pollution in urban areas of Nanjing. The O_3 concentrations are also lower in tunnels, which is associated with the lack of sunlight in the tunnel.

Table 2. Multi-pollutant concentrations in five types of roads.

Road types	Road numbers	Vehicle speed, km/h	Traffic congestion index [a]	CO, mg/m^3	NO_2, μg/m^3	O_3, μg/m^3
Highways	168	60~80	2.18	1.10 ±0.594	29.2 ±8.66	23.3 ±9.12
Arterials	443	40~60	1.78	0.958 ±0.309	25.0 ±6.90	29.7 ±7.53
Secondary	419	30~50	1.70	0.855 ±0.401	21.8 ±8.89	31.9 ±10.0
Branch roads	349	20~40	-	0.818 ±0.216	20.3 ±6.79	32.7 ±12.2
Residential	152	< 20	-	0.783 ±0.230	19.6 ±8.35	35.1 ±15.5

a: The traffic congestion index data is from Gaud map https://report.amap.com/detail.do?city=320100.

https://doi.org/10.5194/acp-2020-1169
Preprint. Discussion started: 24 November 2020

Atmospheric Chemistry and Physics Discussions

3.5 Temporal variation

Figure 8 shows the temporal variation of the three air pollutant concentrations during the observation campaign, with the hourly mean concentrations over the research domain shown in Figure 9 (the corresponding spatial distributions are shown in Figure S2-4). We find that the median concentrations of CO and NO_2 in rush hours (7-9 AM and 5-7 PM) are increased by 26.4% and 27.3% compared to non-rush hours, respectively. The hourly mean concentrations of CO and NO_2 show a double-peak pattern with higher concentrations in rush hours (Figure 9a), reflecting the contribution of traffic-related emissions (Tan et al., 2009), which we will elaborate in next section. The observed O_3 concentrations show a unimodal diurnal pattern with a peak at ~2 PM as a result of photochemical formation. At night, O_3 concentrations are maintained at a low level due to no solar radiation and NOx titration (Xie et al., 2016). These patterns generally agree with the measurements at stationary monitoring stations (Figure S1).

No significant differences are observed for the median concentrations and spatial distribution of three air pollutants between weekdays and weekends ($\alpha = 0.05$, Figure 8b and S3), even though the morning peaks for CO is slightly higher during weekdays (Figure 9b). This might be attributed to the different weekly routine of human activities (Xie et al., 2016) and the randomness of taxi driving trajectory. The median concentrations of CO and NO_2 during holidays are comparable to those in non-holidays, but are 18.3% lower for O_3 (Figure 8c). In addition, compared with the spatial distribution of O_3 concentration in holidays, we find that the concentrations of O_3 in Xinjiekou and its surrounding areas, where many shopping malls are located, are higher in non-holidays (Figure S4). This may be related to the higher NOx concentrations in this area during holidays (24.8±10.2 μg/m^3) than non-holidays (20.6±4.82 μg/m^3). The hourly concentrations show no significant difference between holidays and non-holidays (Figure 9c). The holidays include the periods of National Day (Oct. 1-7), the Spring Festival (Feb. 24-31), Qingming Festival (Apr. 4-6), international labor day (May. 1-5), and the Dragon Boat Festival (Jun. 25-27). "Holiday effect" has been observed extensively for urban and regional air quality. For example, Xu et al. (2017) found that VOC tracers were significantly enhanced during the National Day holiday (from Oct 1 to Oct 10, 2014) in Yangtze River Delta (YRD) region, indicating that the "holiday effect" had a strong influence on the distribution and chemical reactivity of VOC in the atmosphere. The reason why this effect is not observed in this study may be related to the relatively smaller sample size during holidays. The sample size for holidays account for only 11.3% of those for the non-holidays.

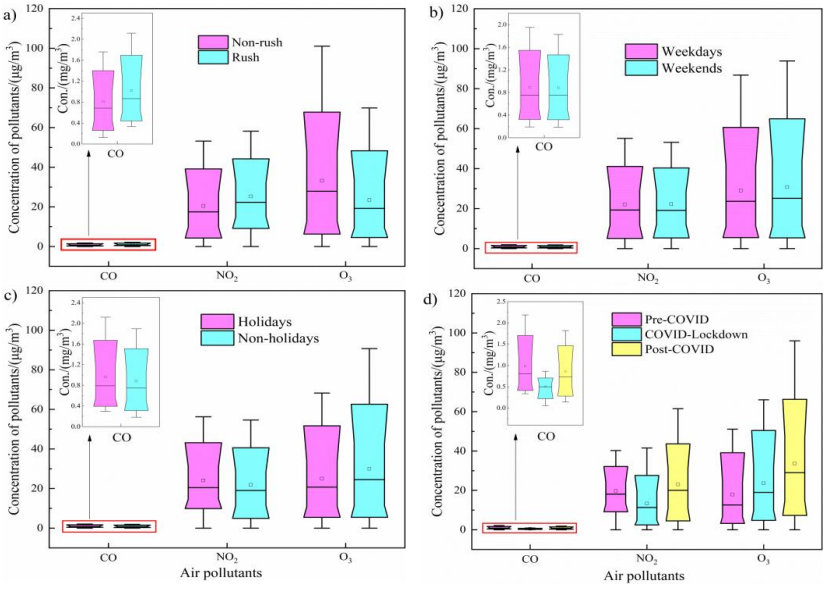

https://doi.org/10.5194/acp-2020-1169
Preprint. Discussion started: 24 November 2020

Atmospheric Chemistry and Physics Discussions

Figure 8. Variation of pollutants concentrations in rush/non-rush hours, weekdays/weekend days, holidays/non-holidays, and three stages of the COVID-19 pandemic. The dot in each box represents the mean value and the solid line represents the median value. Each box extends from the 25th to the 75th percentile. The whiskers (error bars) below and above the boxes represents the 10th and 90th percentiles.

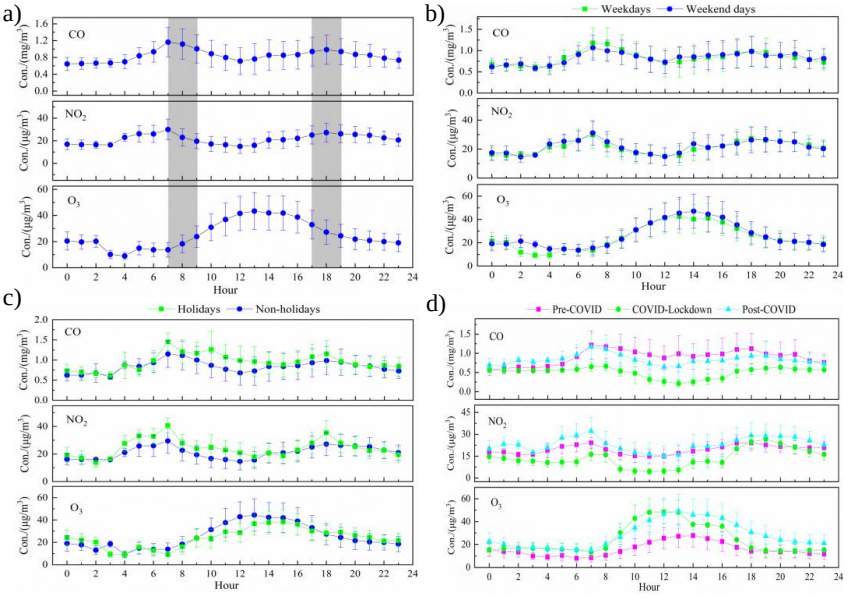

Figure 9. Diurnal cycles of three pollutants concentrations measured in rush/non-rush hours, weekdays/weekend days, holidays/non-holidays, and different stage of the COVID-19 pandemic by the taxi sensors. Error bars in panel a show the standard deviation of observations. Gray areas represent the rush hours, and the other represents the non-rush hours.

3.6 Traffic source contribution

Figure 10a and 10b show the calculated contributions by traffic-related sources to the observed concentrations of CO (referred to as contributions hereinafter). We find that the mean contribution calculated by BS method (42.6±11.5%) is generally consistent with that obtained from PD algorithm (43.9±27.0%). Their spatial patterns are also similar (Figure 10a vs 10b). The contributions in highways, near tunnel entrances and exits (e.g. Jiuhuashan and Xuanwuhu tunnel), railway station (Nanjing south station), and arterial roads (44-59%) calculated by the both methods are higher than secondary roads, residential streets, and lowest in branch roads (29-39%) (Table 3), which is consistent with the trends in traffic volumes. The patterns for NO_2 are quite similar to CO (Figure 10c and 10d, Table 1), but the mean contribution to NO_2 calculated by BS method (26.3±14.7%) is lower than that obtained from PD algorithm (40.2±29.9%). This difference is associated with the relatively higher uncertainty for NO_2 measurements by sensors (Section 2.2), while the results of PD method seem unaffected as the sensor bias are cancelled when calculating the difference between "peak" and "basement" (Section 2.4).

The calculations of the contributions for O_3 are more complex due to its secondary formation. O_3 have lower traffic-related contribution calculated by BS (19.7±15.4%) and PD (30.7±28.2%) methods than CO and NO_2 (Figure S2). The BS method calculates negative values for many residential roads (i.e. background sites have higher O_3 than on some roads, Table 2), indicating the effect of NOx titration and secondary production of O_3 downwind of roads (Li et al., 2013). However, the PD method continues to give positive values in these grids (as, apparently, the "peak" is always higher than "baseline"), which we consider as an artifact. We argue that the difference between the peak and baseline is more reflected by the influence of meteorological factors and chemical reactions, but not traffic-related source contributions for O_3. This indicates the limitations of PD method in determining the contributions of traffic-related sources for secondary pollutants such as O_3.

Bottom-up emission inventory indicates that on-road transportation contributed ~11% of total CO emissions from Nanjing

https://doi.org/10.5194/acp-2020-1169
Preprint. Discussion started: 24 November 2020

Atmospheric Chemistry and Physics Discussions

in 2012 (Zhao et al., 2015). Considering the number of cars has increased ~80% and the total CO emissions remained relatively stable (BSNM, 2019), the contribution of traffic sources in recent years is expected to be ~20%. These values are much lower than what we calculated based on mobile monitoring data because of the lower spatial resolution of these regional inventories (e.g. 0.05°×0.05°) (Zheng et al., 2014). They are unable to distinguish the emission characteristics of air pollutants within a street level (tens of meters), which leads to their underestimation of traffic-related emissions in the road micro-environment.

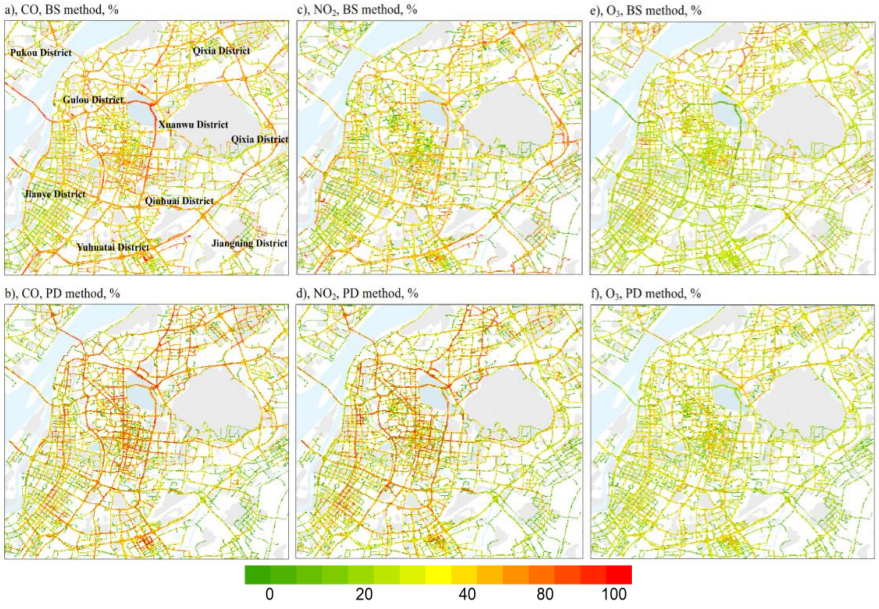

Figure 10. Contributions from traffic-related emissions calculated by stationary data method (a, c, e) and peak detection algorithm (b, d, f) for CO (a, b), NO_2 (c, d), and O_3 (e, f). © OpenStreetMap contributors 2019. Distributed under a Creative Commons BY-SA License.

Table 3. Contribution of traffic emissions to CO, NO_2, and O_3 in different roads by two methods.

Road types	Traffic emission - CO, %		Traffic emission - NO_2, %		Traffic emission - O_3, %	
	BS	PD	BS	PD	BS	PD
Highways	48.3 ±10.4	51.0 ±20.4	32.5 ±14.5	41.4 ±22.5	19.2 ±12.0	32.1 ±27.6
Arterials	44.1 ±9.23	59.0 ±19.4	26.8 ±10.6	43.6 ±23.3	17.6 ±11.9	35.0 ±26.2
Secondary	40.2 ±11.7	47.6 ±23.9	22.8 ±13.2	35.2 ±25.1	21.0 ±13.8	31.2 ±26.6
Residential	39.4 ±14.1	38.9 ±26.1	20.3 ±16.3	28.6 ±25.0	21.9 ±14.7	27.8 ±25.6
Branch roads	39.2 ±12.2	29.7 ±23.9	21.5 ±18.1	25.5 ±24.4	24.1 ±16.5	23.5 ±25.7

3.7 Impact of COVID-19 pandemic

Figure 8d and 9d show the variation of air pollutant concentrations in different stages of the COVID-19 pandemic. The spatial distributions of concentrations and traffic contributions are also depicted in Figure 11 and 12. We divide the data into three stages: Pre-COVID (P1, Oct. 1, 2019 – Jan. 23, 2020), COVID-Lockdown (P2, Jan. 24 – 31, 2020 and Feb. 17 – 24, 2020), and Post-COVID (P3, Mar. 1, 2020 – Sep. 30, 2020). We find the median concentrations of CO and NO_2 were the lowest in P2 (Figure 9d). For example, the CO and NO_2 concentrations decreased by 44.9% and 47.1% from P1 to P2, respectively (Figure 11). This pattern agrees well with the air quality station data over eastern China (Huang et al., 2020). We focus on the traffic sector as it is the most sensitive to lockdown measures, while other sectors, including power, industrial and residential sectors, remain relatively unchanged (Guevara et al., 2020). We find that from P1 to P2, the average traffic source contributions of CO and NO_2 by BS method decreased by 59.9% and 51.8%, respectively (Figure 12). This is consistent with

https://doi.org/10.5194/acp-2020-1169
Preprint. Discussion started: 24 November 2020

Atmospheric Chemistry and Physics Discussions

the transportation index data, which shows a 70% reduction in eastern China cities during lockdown (Huang et al. 2020).

The observed CO and NO_2 concentrations recovered to levels similar to P1 during P3. The traffic-related source contributions were increased by 120% and 131% from P2 to P3 for CO and NO_2 (Figure 11). Due to the limited data size and spatial coverage (only in some arterial roads and highways) during P2, the calculated contributions of traffic emissions to air pollutants may be not directly comparable to those shown in Figure 10. But the changes of the contributions well track the change of traffic volume and human activities (Bao and Zhang, 2020). Our results also agree with top-down emission estimates from remote sensing data (Zhang et al. 2020), which showed the total NO_X emissions decreased by 31-44% from P1 to P2, but increased 67-85% from P2 to P3.

The observed ozone concentrations show a different trend from other pollutants in the three stages. We find a pattern of P1 < P2 < P3 for O_3 median concentrations (Figure 8d). The ozone concentrations increased by 35.7% from P1 to P2, and 48.7% from P2 to P3 (Figure 11). While the contribution of traffic emissions to ozone first decreased by 32.5% from P1 to P2 period, and then increased by 39.3% in P2 to P3 period. This is firstly associated with the less titration of NOx during P2 as discussed earlier. In addition, the increased temperature and solar insulation in P2 and P3 also favor the photochemical formation of O_3 than in P1 (Stathopoulou et al., 2008).

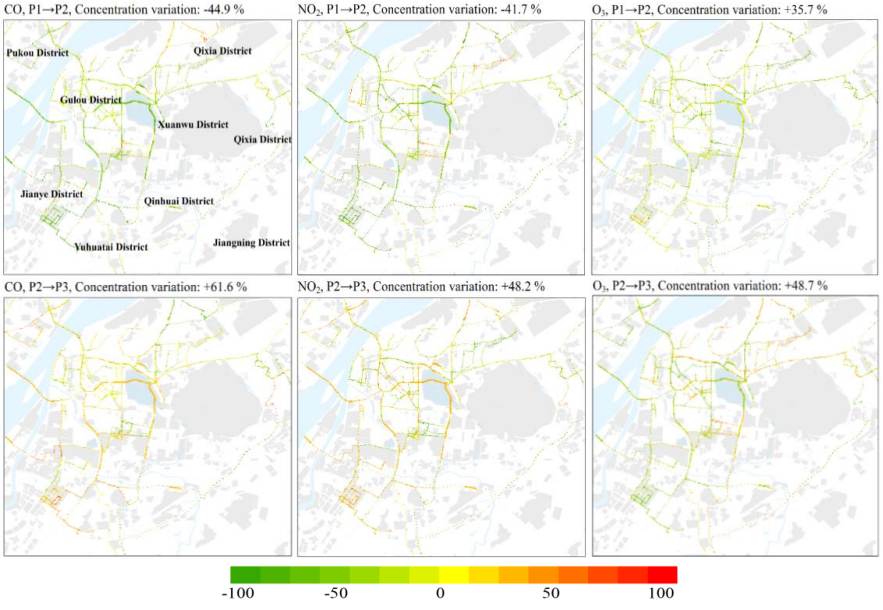

Figure 11. Changes of observed CO, NO_2, and O_3 concentrations in the three stages of the COVID-19 pandemic. P1, P2, and P3 are for pre-COVID, COVID-Lockdown, and post-COVID periods, respectively. © OpenStreetMap contributors 2019. Distributed under a Creative Commons BY-SA License.

https://doi.org/10.5194/acp-2020-1169
Preprint. Discussion started: 24 November 2020

Atmospheric Chemistry and Physics Discussions

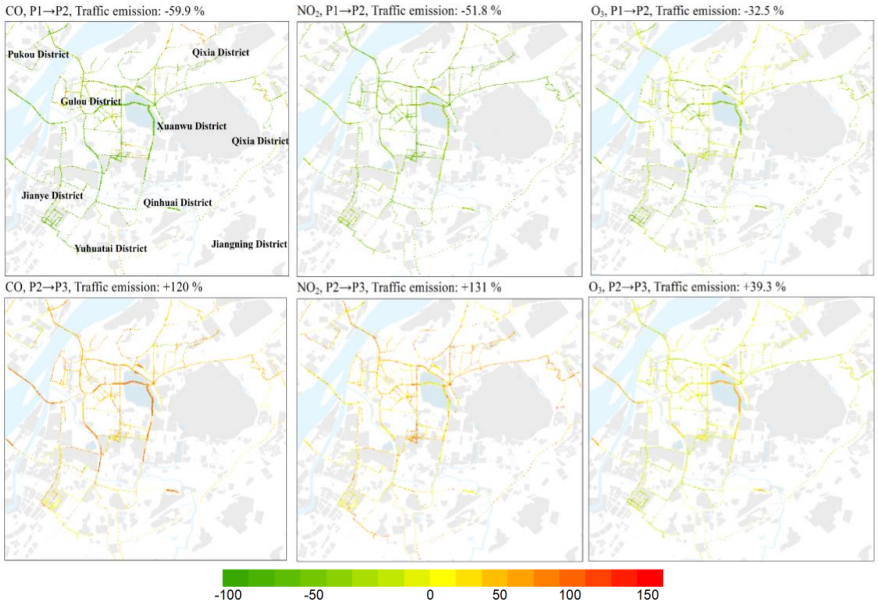

Figure 12. Changes of the contributions of traffic-related sources to CO, NO2, and O3 in the three stages of the COVID-19 pandemic calculated by BS method. P1, P2, and P3 are for pre-COVID, COVID-Lockdown, and post-COVID periods, respectively. © OpenStreetMap contributors 2019. Distributed under a Creative Commons BY-SA License.

4 Conclusions

To accurately assess human exposure to urban air pollution requires a detailed understanding of the spatial and temporal patterns of air pollutant concentrations. Combined mobile monitoring with GIS technology, we obtained high-resolution (50m×50m) spatial distribution maps of three air pollutants in the main urban area of Nanjing, which well demonstrates the spatial heterogeneity of pollutants at the micro-scales. We find that higher spatial resolutions are useful to identify hotspots that are mainly affected by five types of air pollution source emissions, namely, traffic, industrial, dust, and cooking fumes. It also provides hints for air quality management and emission source control.

We calculate the contribution of traffic-related emissions to air pollutants in different grid points by combining mobile observation and station observation data. Compared with the peak detection method, the station data method is more reasonable for secondary pollutants as O_3, while the former is less affected by sensor bias. There are also differences in the contribution of traffic emissions to air pollutants in different types of roads. Due to the impact of the COVID-19 pandemic, the mean concentrations of CO and NO_2 decreased by 44.9% and 47.1%, respectively, during the lockdown in Nanjing, and the contribution of traffic-related emissions also decreased by 59.9% and 52.6%. On the contrary, the concentration of O_3 increased by 35.7%, respectively. After reopening, CO and NO_2 concentrations rebounded by 61.6% and 48.2%, and the contribution of traffic emissions both increased over 100%, indicating the great impact of traffic emissions on urban air pollution.

Data availability

All validation data and data processing by GIS used in this work are accessed by contacting the authors.

Author contribution

YZ designed the research; SW performed the research; SW, YZ, ZW, and MY analyzed data; LW, XC, and AD provided validation data; MY, YL, and QL helped data analysis; MW, LZ, and YX provided monitoring instrument; SW and YZ wrote the paper.

https://doi.org/10.5194/acp-2020-1169
Preprint. Discussion started: 24 November 2020

365

Competing interests

The authors declare that they have no conflict of interest.

Acknowledgments

This study was supported by the National Key R&D Program of China (2019YFA0606803), Start-up fund of the Thousand
370 Youth Talents Plan, Jiangsu Innovative and Entrepreneurial Talents Plan, and the Collaborative Innovation Center of Climate Change, Jiangsu Province. The authors thank Rong Ye and Liang Luo for sample collection.

References

Airparif.: Influence des aménagements de voirie sur l'exposition des cyclists a la pollution atmospherique; Study report Airparif: Paris, France, 2009.

375 Apte, J. S., Messier, K. P., Gani, S., Brauer, M., Kirchstetter, T. W., Lunden, M. M., Marshall, J. D., Portier, C. J., Vermeulen, R. C. H., and Hamburg, S. P.: High-resolution air pollution mapping with google street view cars: exploiting big data, Environ. Sci. Technol., 51, 6999-7008, https://doi.org/10.1021/acs.est.7b00891, 2017.

Apte, J. S., Kirchstetter, T. W., Reich, A. H., Deshpande, S. J., Kaushik, G., Chel, A., Marshall, J. D., and Nazaroff, W. W.: Concentrations of fine, ultrafine, and black carbon particles in auto-rickshaws in New Delhi, India, Atmos. Environ., 45,
380 4470-4480, https://doi.org/10.1016/j.atmosenv.2011.05.028, 2011.

Bao, R. and Zhang, A.: Does lockdown reduce air pollution? Evidence from 44 cities in northern China, Sci. Total Environ., 139052, https://doi.org/10.1016/j.scitotenv.2020.139052, 2020.

Bart, E., Jan P., Martine, V. P., Nico, B., and Arnout, S.: The aeroflex: a bicycle for mobile air quality measurements, Sensors, 13(1), 221-240, https://doi.org/10.3390/s130100221, 2012.

385 Boogaard, H., Kos, G. P. A., Weijers, E. P., Janssen, N. A. H., Fischer, P. H., Van der Zee, S. C., De Hartog, J. J., and Hoek, G.: Contrast in air pollution components between major streets and background locations: Particulate matter mass, black carbon, elemental composition, nitrogen oxide and ultrafine particle number, Atmos. Environ., 45, 650-658, https://doi.org/10.1016/j.atmosenv.2010.10.033, 2010.

Borrego, C., Coutinho, M., Costa, A. M., Ginja, J., Ribeiro, C., Monteiro, A., Ribeiro, I., Valente, J., Amorim, J. H., Martins,
390 H., Lopes, D., and Miranda, A. I.: Challenges for a new air quality directive: the role of monitoring and modelling techniques, Urban Climate, 14 (3), 328-341, https://doi.org/10.1016/j.uclim.2014.06.007, 2015.

Bossche, J. V. D., Peters, J., Verwaeren, J., Botteldooren, D., Theunis, J., and Baets, B. D.: Mobile monitoring for mapping spatial variation in urban air quality: Development and validation of a methodology based on an extensive dataset, Atmos. Environ., 105, 148-161, https://doi.org/10.1016/j.atmosenv.2015.01.017, 2015.

395 Bureau Statistics of Nanjing Municipal.: Nangjing Statistical Yearbook. http://tjj.nanjing.gov.cn/tjxx/202004/t20200407_1828594.html, 2019.

Castell, N., Dauge, F. R., Schneider, P., Vogt, M., Lerner, U., Fishbain, B., Broday, D., and Bartonova, A.: Can commercial low-cost sensor platforms contribute to air quality monitoring and exposure estimates? Environ. Int., 99, 293-302, https://doi.org/10.1016/j.envint.2016.12.007, 2017.

400 Cavellin, L. D., Weichenthal, S., Tack, R., Ragettli, M. S., Smargiassi, A., and Hatzopoulou, M.: Investigating the use of portable air pollution sensors to capture the spatial variability of traffic-related air pollution, Environ. Sci. Technol., 50, 313 320, https://doi.org/10.1021/acs.est.5b04235, 2016.

Chatzidiakou, L., Krause, A., Popoola1, O. A. M., Antonio1, A.D., Kellaway, M., Han, Y.Q., Squires, F. A., Wang, T., Zhang, H. B., Wang, Q., Fan, Y. F., Chen, S. Y., Hu, M., Quint, J. K., Barratt, B., Kelly, F. J., Zhu, T., and Jones, R. L.: Characterising

https://doi.org/10.5194/acp-2020-1169
Preprint. Discussion started: 24 November 2020

Atmospheric Chemistry and Physics Discussions

low-cost sensors in highly portable platforms to quantify personal exposure in diverse environments, Atmos. Meas. Tech., 12, 4643-4657, https://doi.org/10.5194/amt-12-4643-2019, 2019.

Ding, A. J., Fu, C. B., Yang, X. Q., Sun, J. N., Zheng, L. F., Xie, Y. N., Herrmann, E., Nie, W., Petäjä, T., Kerminen, V. -M., and Kulmala M.: Ozone and fine particle in the western Yangtze River Delta: an overview of 1 yr data at the SORPES station, Atmos. Chem. Phys., 13, 5813-5830, https://doi.org/10.5194/acp-13-5813-2013, 2013.

Farrell, W. J., Cavellin, L. D., Weichenthal, S., Goldberg, M., and Hatzopoulou, M.: Capturing the urban canyon effect on particle number concentrations across a large road network using spatial analysis tools, Build. Environ., 92, 328-334, https://doi.org/10.1016/j.buildenv.2015.05.004, 2015.

Gately, C. K., Hutyra, L. R., Peterson, S., and Wing, I. S.: Urban emissions hotspots: Quantifying vehicle congestion and air pollution using mobile phone GPS data, Environ. Pollut., 229, 496-504, https://doi.org/10.1016/j.envpol.2017.05.091, 2017.

Guevara, M., Jorba, O., Soret, A., Petetin, H., Bowdalo, D., Serradell, K., Tena, C., Van der Gon, H. D., Kuenen, J., Peuch, V. H., and García-Pando, C. P.: Time-resolved emission reductions for atmospheric chemistry modelling in Europe during the COVID-19 lockdowns, Atmos. Chem. Phys., doi.org/10.5194/acp-2020-686, 2020.

Hagan, D. H., Gani, S., Bhandari, S., Patel, K., Habib, G., Apte, J. S., Ruiz, L. H., and Kroll, J. H.: Inferring aerosol sources from low-cost air quality sensor measurements: a case study in Delhi, India, Environ, Sci. Technol. Lett., 6, 467-472, https://doi.org/10.1021/acs.estlett.9b00393, 2019.

Hasenfratz, D., Saukh, O., Walser, C., Hueglin, C., Fierz, M., Arn, T., Beutel, J., and Thiele, L.: Deriving high-resolution urban air pollution maps using mobile sensor nodes, Pervasive and Mobile Computing, 16, 268-285, https://doi.org/10.1016/j.pmcj.2014.11.008, 2015.

Hilker, N., Wang, J. M., Jeong, C., Healy, R. M., Sofowote, U., Debosz, J., Su, Y., Noble, M., Munoz, A., Doerksen, G., White, L., Audette, C., Herod, D., Brook, J. R., and Evans, G. J.: Traffic-related air pollution near roadways: discerning local impacts from background, Atmos. Meas. Tech., 12, 5247-5261, https://doi.org/10.5194/amt-12-5247-2019, 2019.

Huang, X., Ding, A. J., Gao, J., Zheng, B., Zhou, D. R., Qi, X., Tang, R., Wang, J., Ren, C., Nie, W., Chi, X., Xu, Z., Chen, L., Li, Y., Che, F., Pang, N., Wang, H. K., Tong, D., Qin, W., Cheng, W., Liu, W., Fu, Q., Liu, B., Chai, F. H., Davis, S. J., Zhang, Q., and He, K. B.: Enhanced secondary pollution offset reduction of primary emissions during COVID-19 lockdown in China, Natl. Sci. Rev., https://doi.org/10.1093/nsr/nwaa137, 2020.

Isakov, V., Touma, J. S., and Khlystov, A.: A method of assessing air toxics concentrations in urban areas using mobile platform measurements, J. Air Waste Manage. Assoc., 57(11), 1286-1295, https://doi.org/10.3155/10473289.57.11.1286, 2007.

Johnson, N. E., Bonczak, B., and Kontokosta, C. E.: Using a gradient boosting model to improve the performance of low-cost aerosol monitors in a dense, heterogeneous urban environment, Atmos. Environ., 184, 9-16, https://doi.org/10.1016/j.atmosenv.2018.04.019, 2018.

Kaivonen, S. and Ngai, E.: Real-time air pollution monitoring with sensors on city bus, Digit. Commun. Netw., 6, 23-30, https://doi.org/10.1016/j.dcan.2019.03.003, 2020.

Karner, A. A., Eisinger, D. S., and Niemeier, D. A.: Near-roadway air quality: synthesizing the findings from real-world data, Environ. Sci. Technol., 44(14), 5334-5344, https://doi.org/10.1021/es100008x, 2010.

Kaur, S., Nieuwenhuijsen, M. J., and Colvile, R. N.: Fine particulate matter and carbon monoxide exposure concentrations in urban street transport microenvironments, Atmos. Environ., 41, 4781-4810, https://doi.org/10.1016/j.atmosenv.2007.02.002, 2007.

Kerckhoffs, J., Hoek, G., Messier, K. P., Brunekreef, B., Meliefste, K., Klompmaker, J. O., and Vermeulen, R.: Comparison of ultrafine particle and black carbon concentration predictions from a mobile and short-term stationary land-use regression model, Environ. Sci. Technol., 50(23), 12894-12902, https://doi.org/10.1021/acs.est.6b03476, 2016.

Laughner, J. L., Zhu, Q., and Cohen, R. C.: The berkeley high resolution tropospheric NO_2 product, Earth Syst. Sci., Data 10, 2069-2095, https://doi.org/10.5194/essd-10-2069-2018, 2018.

https://doi.org/10.5194/acp-2020-1169
Preprint. Discussion started: 24 November 2020

Atmospheric Chemistry and Physics Discussions

Le, D. K. and Cha, S. K.: Real-time Air Pollution prediction model based on Spatiotemporal Big data, Computers and Society, https://arxiv.org/ftp/arxiv/papers/1805/1805.00432.pdf, 2018.

Li, M. J., Chen, D. S., Cheng, S. Y., Wang, F., Li, Y., Zhou, Y., and Lang, J. L.: Optimizing emission inventory for chemical transport models by using genetic algorithm, Atmos. Environ., 44(32), 3926-3934, https://doi.org/10.1016/j.atmosenv.2010.07.010, 2010.

Li, Y., Lau, A.K.H., Fung, J. C. H., Zheng, J. Y., and Liu, S.: Importance of NOx control for peak ozone reduction in the Pearl River Delta region, Journal of Geophysical Research: Atmospheres, 118, 9428-9443, https://doi.org/10.1002/jgrd.50659, 2013. Li, Z., Fung, J. C. H., and Lau, A. K. H.: High spatiotemporal characterization of on-road $PM_{2.5}$ concentrations in high-density urban areas using mobile monitoring, Build. Environ., 143, 196-205, https://doi.org/10.1016/j.buildenv.2018.07.014, 2018.

Lim, C. C., Kim, H., Vilcassim, M. J. R., Thurston, G. D., Gordon, T., Chen, L. C., Lee, K., Heimbinder, M., and Kim, S.: Mapping urban air quality using mobile sampling with low-cost sensors and machine learning in Seoul, South Korea, Environ. Int., 131, 105022, https://doi.org/10.1016/j.envint.2019.105022, 2019.

McClurkin, J. D., Maier, D. E., and Ileleji, K. E.: Half-life time of ozone as a function of air movement and conditions in a sealed container, Journal of Stored Products Research, 55, 41-47, https://doi.org/10.1016/j.jspr.2013.07.006, 2013.

Miller, D. J., Actkinson, B., Padilla, L., Griffin, R. J., Moore, K., Lewis, P. G. T., Gardner-Frolick, R., Craft, E., Portier, C. J., Hamburg, S. P., and Alvarez, R.A.: Characterizing elevated urban air pollutant spatial patterns with mobile monitoring in Houston, Texas, Environ. Sci. Technol., 54(4), 2133-2142, https://doi.org/10.1021/acs.est.9b05523, 2020.

Ministry of Ecology and Environment of the People's Republic of China.: 2018 China Vehicle Environmental Management Annual Report. retrieved from http://www.mee.gov.cn/xxgk2018/xxgk/xxgk15/201806/t20180601_630215.html, 2018.

Miskell, G., Salmond, J., and Williams, D. E.: A solution to the problem of calibration of low-cost air quality measurement sensors in networks, Acs. Sensors, 3, 832-843, https://doi.org/10.1021/acssensors.8b00074, 2018.

OpenStreetMap contributors: Roads and land use data of Nanjing retrieved from https://download.geofabrik.de/asia/china.html, https://www.openstreetmap.org, 2020.

Padro-Martinez, L. T., Patton, A. P., Trull, J. B., Zamore, W., Brugge, D., and Durant, J. L.: Mobile monitoring of particle number concentration and other traffic-related air pollutants in a near-highway neighborhood over the course of a year, Atmos. Environ., 61, 253-264, https://doi.org/10.1016/j.atmosenv.2012.06.088, 2012.

Peters, J., Theunis, J., Van Poppel, M., and Berghmans, P.: Monitoring PM_{10} and ultrafine particles in urban environments using mobile measurements, Aerosol Air Qual. Res., 13, 509-522, doi.org/10.4209/aaqr.2012.06.0152, 2013.

Poppel, M. V., Peters, J., and Bleux, N.: Methodology for setup and data processing of mobile air quality measurements to assess the spatial variability of concentrations in urban environments, Environ. Pollut., 183, 224-233, https://doi.org/10.1016/j.envpol.2013.02.020, 2013.

Romer, P. S., Duffey, K. C., Wooldridge, P. J., Allen, H. M., Ayres, B. R., Brown, S. S., Brune, W. H., Crounse, J. D., Gouw, J. D., Draper, D. C., Feiner, P. A., Fry, J. L., Goldstein, A. H., Koss, A., Misztal, P. K., Nguyen, T. B., Olson, K., Teng, A. P., Wennberg, P. O., Wild, R. J., Zhang, L., and Cohen, R. C.: The lifetime of nitrogen oxides in an isoprene-dominated forest, Atmos. Chem. Phys., 16, 7623-7637, http://doi.org/10.5194/acp-16-7623-2016, 2016.

Sharma, S., Sharma, P., Khare, M., and Kwatra, S.: Statistical behavior of ozone in urban environment, Sust. Environ. Res., 26 (3), 142-148, https://doi.org/10.1016/j.serj.2016.04.006, 2016.

Shiva, N. S. M., Pavan, R.Y., Narayana, M. V., Seema, K., and Pooja, R.: Mobile monitoring of air pollution using low cost sensors to visualize spatio-temporal variation of pollutants at urban hotspots, Sustainable Cities and Society, 44, 520-535, https://doi.org/10.1016/j.scs.2018.10.006, 2019.

Snyder, E. G., Watkins, T. H., Solomon, P. A., Thoma, E. D., Williams, R. W., Hagler, G. S. W., Shelow, D., Hindin, D. A., Kilaru, V. J., and Preuss, P. W.: The changing paradigm of air pollution monitoring, Environ. Sci. Technol., 47 (20), 11369-

11377, https://doi.org/10.1021/es4022602, 2013.

Spinelle, L., Gerboles, M., Villani, M., Aleixandre, M., and Bonavitacola, F.: Field calibration of a cluster of low-cost commercially available sensors for air quality monitoring. Part B: NO, CO and CO_2, Sensors Actuators B Chem., 238, 706-715, https://doi.org/10.1016/j.snb.2016.07.036, 2017.

Stathopoulou, E., Mihalakakou, G., Santamouris, M., and Bagiorgas, H. S.: On the impact of temperature on tropospheric ozone concentration levels in urban environments, J. Earth Syst. Sci., 117, 227-223, https://doi.org/10.1007/s12040008002 79, 2008.

Tan, P. H., Chou, C., Liang, J. Y., Chou, C. C. K., and Shiu, C. J.: Air pollution "holiday effect" resulting from the Chinese New Year, Atmos. Environ., 43(13), 2114-2124, https://doi.org/10.1016/j.atmosenv.2009.01.037, 2009.

Targino, A. C., Gibson, M. D., Krecl, P., Rodrigues, M. V. C., Santos, M. M. D., and Corrêa, M. D. P.: Hotspots of black carbon and $PM_{2.5}$ in an urban area and relationships to traffic characteristics, Environ. Pollut., 218, 475-486, https://doi.org/10.1016/j.envpol.2016.07.027, 2016.

Wei, P., Ning, Z., Ye, S., Sun, L., Yang, F., Wong, K. C., Westerdahl, D., Louie, P.: Impact analysis of temperature and humidity conditions on electrochemical sensor response in ambient air quality monitoring, Sensors (Basel, Switzerland), 18(2), 59, doi.org/10.3390/s18020059, 2018.

Weissert, L., Alberti, K., Miles, E., Miskell, G., Feenstra, B., Henshaw, G. S., Papapostolou, V., Patel, H., Polidori, A., Salmond, J. A., and Williams, D. E.: Low-cost sensor networks and land-use regression: Interpolating nitrogen dioxide concentration at high temporal and spatial resolution in Southern California, Atmos. Environ., 223, 117287, doi.org/10.1016/j.atmosenv.2020.117287, 2020.

World Health Organization, 2016. WHO Global Urban Ambient Air Pollution Database. Available at: https://www.who.int/phe/health_topics/outdoorair/databases/cities/en/, Accessed date: May 4, 2020.

World Health Organization, May 2, 2018. 9 out of 10 People Worldwide Breathe Polluted Air, but More Countries Are Taking Action. Available at. https://www.who.int/news-room/detail/02-05-2018-9-out-of-10-people-worldwide-breathe-polluted-airbut-more-countries-are-taking-action, Accessed date: 16 September 2018.

Wu, Y., Zhang, S., Hao, J. M., Liu, H., Wu, X., Hu, J. N., Walsh, M. P., Wallington, T. J., Zhang, K. M., and Stevanovic, S.: On-road vehicle emissions and their control in China: a review and outlook, Sci. Total Environ., 574, 332-349, https://doi.org/10.1016/j.scitotenv.2016.09.040, 2017.

Xie, M., Zhu, K., Wang, T., Chen, L., Han, Y., Li, S., Zhuang, B. L., and Shu, L.: Temporal characterization and regional contribution to O_3 and NOx at an urban and a suburban site in Nanjing, China. Sci. Total Environ., 551-552, 533-545, https://doi.org/10.1016/j.scitotenv.2016.02.047, 2016.

Xie, Y., Zhao, B., Zhang, L., and Luo, R.: Spatiotemporal variations of $PM_{2.5}$ and PM_{10} concentrations between 31 Chinese cities and their relationships with SO_2, NO_2, CO and O_3, Particuology. 20, 141-149, https://doi.org/10.1016/j.partic.2015.01.003, 2015.

Xu, H., Bechle, M. J., Wang, M., Szpiro, A. A., Vedal, S., Bai, Y. Q., and Marshall, J. D.: National $PM_{2.5}$ and NO_2 exposure models for China based on land use regression, satellite measurements, and universal kriging, Sci. Total Environ., 655, 423-433, https://doi.org/10.1016/j.scitotenv.2018.11.125, 2019.

Xu, Z., Huang, X., Nie, W., Chi, X., Xu, Z., Zheng, L., Sun, P., and Ding, A. J.: Influence of synoptic condition and holiday effects on VOCs and ozone production in the Yangtze River Delta region, China, Atmos. Environ., 168, 112-124, https://doi.org/10.1016/j.atmosenv.2017.08.035, 2017.

Zhang, H., Xu, T., Zong, Y., Tang, H., Liu, X., and Wang, Y. C.: Influence of meteorological conditions on pollutant dispersion in street canyon, Procedia Engineering, 121, 899-905, https://doi.org/10.1016/j.proeng.2015.09.047, 2015.

Zhang, R., Zhang, Y., Lin, H., Feng, X., Fu, T. M., and Wang, Y. H.: NOx emission reduction and recovery during COVID-19 in east China, Atmosphere, 11, 433, http://doi:10.3390/atmos11040433, 2020.

https://doi.org/10.5194/acp-2020-1169
Preprint. Discussion started: 24 November 2020

Atmospheric Chemistry and Physics Discussions

Zhang, Y. X, Ye, X. P, Wang, S. B, He, X. J, Dong, L. Y, Zhang, N., Wang, H. K., Wang, Z. R., Ma, Y., Wang, L., Chi, X. G., Ding, A. J., Yao, M. Z., Li, Y. P., Li, Q. L., Zhang, L., and Xiao, Y. L.: Large-eddy simulation of traffic-related air pollution at a very high-resolution in a mega-city: Evaluation against mobile sensors and insights for influencing factors, doi.org/10.31223/osf.io/n2py6, 2020.

Zhao, Y., Qiu, L. P., Xu, R. Y., Xie, F. J., Zhang, Q., Yu, Y. Y., Nielsen, C. P., Qin, H. X., Wang, H. K., Wu, X. C., Li, W. Q., and Zhang, J.: Advantages of a city-scale emission inventory for urban air quality research and policy: The case of Nanjing, a typical industrial city in the Yangtze River Delta, China, Atmos. Chem. Phys., 15, 12623-12644, https://doi.org/10.5194/acp1512623-2015, 2015.

Zheng, B., Huo, H., Zhang, Q., Yao, Z. L., Wang, X. T., Yang, X. F., Liu, H., and He, K. B.: High-resolution mapping of vehicle emissions in China in 2008, Atmos. Chem. Phys., 14, 9787-9805, https://doi.org/10.5194/acp-14-9787-2014, 2014.

Zhu, Y. F., Pudota, J., Collins, D., Allen, D., Clements, A., DenBleyker, A., Fraser, M., Jia, Y. L., McDonald-Buller, E., and Michel, E.: Air pollutant concentrations near three Texas roadways, Part I: Ultrafine particles, Atmos. Environ., 43(30), 4513-4522, https://doi.org/10.1016/j.atmosenv.2009.04.018, 2009.

Zou, C., Wu, L., Li, X., Yuan, Y., Jing, B., and Mao, H. J.: Relationship between traffic flow and temporal and spatial variations of NO_2 and CO in Nanjing, Acta Sci. Circumstantiae., 37(10), 3894-3905, doi.org/10.13671/j.hjkxxb.2017.0374, 2017.